Biogeosciences Discuss., 11, 8373–8397, 2014
www.biogeosciences-discuss.net/11/8373/2014/
doi:10.5194/bgd-11-8373-2014

Biogeosciences Discussions
Open Access

Wind-induced upwelling in the Kerguelen Plateau Region

S. T. Gille[1], M. M. Carranza[1], R. Cambra[2,*], and R. Morrow[2]

[1]Scripps Institution of Oceanography, University of California, San Diego, USA
[2]Laboratoire d'Etudes en Géophysique et Océanographie Spatiale, Observatoire Midi-Pyrénées, 31400 Toulouse, France
[*]now at: Laboratoire Atmosphères, Milieux, Observations Spatiales, Institute Pierre-Simon Laplace, Paris, France

Received: 14 May 2014 – Accepted: 17 May 2014 – Published: 5 June 2014

Correspondence to: S. T. Gille (sgille@ucsd.edu)

Published by Copernicus Publications on behalf of the European Geosciences Union.

Abstract

In contrast to most of the Southern Ocean, the Kerguelen Plateau supports an unusually strong spring chlorophyll (Chl *a*) bloom, likely because the euphotic zone in the region is supplied with higher iron concentrations. This study uses satellite wind, sea surface temperature (SST), and ocean color data to explore the impact of wind-driven processes on upwelling of cold (presumably iron-rich) water to the euphotic zone. High wind speeds typically correlate with cold sea surface temperatures, implying that wind-mixing leads to enhanced vertical mixing. Negative wind-stress curl also correlates with cold SSTs, implying that Ekman pumping can further enhance upwelling, and coupling between winds and SSTs associated with mesoscale eddies can locally modulate the wind-stress curl. Kerguelen has a significant wind shadow on its downwind side, which generates a wind-stress curl dipole that shifts location depending on wind direction. This leads to locally enhanced Ekman pumping on the downstream side of the Kerguelen Plateau, where Chl *a* blooms are observed most years.

1 Introduction

The Southern Ocean is characterized as a region of high nutrients but low chlorophyll (HNLC), where low concentrations of dissolved iron inhibit growth of phytoplankton, despite the presence of ample quantities of macronutrients (Martin et al., 1990; de Baar et al., 2005; Boyd, 2002). Exceptions to the HNLC regime occur in a few limited areas, primarily near the Antarctic continental shelf (e.g., Moore and Abbott, 2000; Holm-Hansen et al., 2004; Kahru et al., 2007; Arrigo et al., 2008; Frants et al., 2013) or near specific islands (e.g., Blain et al., 2007; Pollard et al., 2007; Planquette et al., 2007; Venables et al., 2007; Korb et al., 2008), where iron can be supplied to surface waters from ocean sediments. The plateau surrounding the Kerguelen Islands supports a particularly strong bloom, which has been the target of two KErguelen Ocean and

BGD
11, 8373–8397, 2014

Plateau compared Study (KEOPS) field campaigns (e.g., Blain et al., 2007, and papers in this volume).

In most of the Southern Ocean, wind forcing is thought to influence seasonal and interannual variations in biological productivity through several competing mechanisms. Strong winds can deepen the mixed layer, bringing up to the euphotic zone cold water that is rich in iron and macronutrients, and thus enhancing phytoplankton growth. In some places, and particularly in low-stratification environments such as commonly occur in the Southern Ocean, strong winds can also deepen the mixed layer enough to mix phytoplankton over large vertical distances, thus reducing average light levels and limiting phytoplankton growth (e.g., Kahru et al., 2010; Fauchereau et al., 2011). Typically along the primary axis of the Antarctic Circumpolar Current (ACC), around 50° S in the Kerguelen region, mean wind stress is a maximum, and wind-stress curl is zero. Depending on the sign of the wind-stress curl, this may play a further role in biological productivity: south of the zero wind-stress curl line, Ekman pumping drives upwelling, which can bring iron and macronutrients up from below the mixed layer, while to the north, Ekman pumping results in downwelling (Carranza and Gille, 2014). While wind mixing and Ekman pumping provide a basic framework for evaluating large-scale processes, at any given location, local effects can significantly modify large-scale wind processes. At eddy-length scales, sea surface temperature (SST) anomalies can modify surface winds, which tend to accelerate over warm water and slow over cool, resulting in local modifications to the wind-stress curl and divergence (e.g., O'Neill et al., 2003, 2005) and correspondingly to the local Ekman pumping velocity. In addition, eddies themselves influence local chlorophyll concentrations, and this may be associated both with horizontal advection induced by the eddies (e.g., Chelton et al., 2011), with eddy influences on upper ocean stratification (e.g., Mahadevan et al., 2012), or from strong vertical velocities induced within the filaments surrounding the eddies (e.g., Lévy et al., 2012).

While wind-driven upwelling appears to play a central role in determining variability in phytoplankton growth in regions of the Southern Ocean that are far from land (e.g.

BGD
11, 8373–8397, 2014

Kahru et al., 2010; Fauchereau et al., 2011; Carranza and Gille, 2014), the role of wind is less clear in areas near islands where phytoplankton blooms are stronger and more persistent and where a broader range of processes might be expected to control iron availability. These processes include oceanic transport processes (which might vary the sediment content of water advected away from the island shelf) as well as local orographic influences on winds. For example, Kerguelen, which stands 1850 m tall, produces a substantial wind shadow, which in turn modifies the wind-stress curl (Chelton et al., 2004). The present study was thus carried out as a complement to the KEOPS-2 field campaign, with the aim to assess the extent to which wind-driven upwelling mechanisms might contribute to the nutrient availability and biological productivity in the region around Kerguelen.

In this study we focus on two key issues. First for the region around Kerguelen, we evaluate the extent to which the wind-stress and wind-stress curl driven mechanisms control sea surface temperature (and by extension nutrients and chlorophyll, as shown in Fig. 1). As part of this analysis, we specifically consider the role that the Kerguelen wind shadow could play in modifying wind-driven upwelling. Second, we evaluate whether wind-driven processes play a significant role in the region around Kerguelen, where a large bloom is present. SST will serve as a proxy for nutrients for much of this analysis. Chlorophyll is more difficult to interpret than SST, because satellite-derived chlorophyll estimates are only available in cloud-free conditions, which are comparatively rare in the Southern Ocean, and because phytoplankton require time to grow after they are first exposed to optimal nutrient and light levels, and thus chlorophyll concentrations can lag physical parameters by an increment of time that has not been determined precisely. However, SST and chlorophyll can also differ in fundamental ways: SST anomalies can influence wind, inducing a coupled air–sea interaction, whereas chlorophyll concentrations do not influence wind. Section 2 discusses the range of satellite data and reanalysis products that we consider for this analysis, Sect. 3 briefly summarizes the computational methodology, Sect. 4 presents the results, and Sect. 5 provides a summary and conclusions.

BGD
11, 8373–8397, 2014

2 Data

Vector wind data were derived from scatterometer measurements obtained by the Quick Scatterometer (QuikSCAT) satellite, which operated from June 1999 through November 2009 (Freilich et al., 1994). We made use of daily and weekly averages of the QuikSCAT Level 4 Gridded Mean Wind Fields produced by L'Institut Français de Recherche pour l'Exploitation de la Mer's Center for Satellite Exploitation and Research (Ifremer/CERSAT). Data are released on a 0.5° regular grid (cersat.ifremer.fr). Since QuikSCAT failed in 2009, for the time period corresponding to the KEOPS-2 field program, we use Cross-Calibrated Multi-Platform (CCMP) winds (Atlas et al., 2008, 2009), which our tests show to be effective at capturing wind variability on time scales as short as the diurnal cycle (Carranza and Gille, 2014).

SST data were obtained from the Advanced Microwave Scanning Radiometer for the Earth Observing System (AMSR-E), which operated from June 2002 through early October 2011 (Chelton and Wentz, 2005). We use version 3 of the objectively interpolated fields distributed by Remote Sensing Systems (RSS). (The SST data fields formally merge measurements from 3 microwave sensors, TMI, AMSR-E, and WindSat, but we consider a latitude range and time period when the fields should be determined only by AMSR-E.) The data are daily averages on a 0.25° grid. Microwave SST data have the advantage of being available in almost all non-precipitating weather conditions, in contrast with infrared SST data, which offer higher spatial resolution but do not return data in cloudy conditions. Clouds are prevalent about 70 % of the time in the mid-latitude regions such as the Southern Ocean (Chelton and Wentz, 2005). For this study, data were analyzed for a 7-year time period from 1 November 2002 through 31 October 2009, chosen to represent an integer number of years and to have both QuikSCAT winds and AMSR-E SSTs available. From this time period, we have omitted 5 isolated days for which wind data were missing from the CERSAT records. Unless otherwise stated, all analyses in this paper were carried out for this full time interval. Figure 1d shows climatological mean SST for spring, and Fig. 1e shows summer SST.

BGD
11, 8373–8397, 2014

As a point of comparison, Fig. 1f shows mean SST from October–November 2011, when the KEOPS-2 field program took place. For 2011, SSTs come from WindSat.

Sea surface geostrophic velocity anomalies (relative to a temporal mean from 1992–1999) were produced by the SSALTO/DUACS project, which computes them based on a multi-satellite altimeter product (Le Traon et al., 1998; Ducet et al., 2000; Dibarboure et al., 2011). These data, which are distributed by AVISO, are released at weekly intervals, and each map uses roughly a two-week window of satellite observations, mapped on a regular Mercator grid with a grid spacing of 0.33° longitude by roughly 0.2° latitude. Eddy kinetic energy (EKE) was computed by first removing the mean for the analysis time period, in order to obtain velocities anomalies u' and v', and then computing EKE = $(u'^2 + v'^2)/2$.

We use net surface heat fluxes from NCEP Climate Forecast System Reanalysis (NCEP/CFSR, Saha et al., 2010). This is a high resolution coupled-global reanalysis that incorporates satellite measurements. Net surface heat flux accuracy increases over time in NCEP/CFSR, showing smaller biases compared to the NCEP/NCAR reanalysis (Saha et al., 2010; Xue et al., 2010). They are available at 1 h and 0.5° × 0.5°, and we spatially interpolated and averaged in time to match the resolution of satellite fields.

Finally, we considered ocean color data as a proxy for chlorophyll *a* (Chl *a*) concentration at the ocean surface. Figure 1a shows climatological spring, and Fig. 1b shows summer Chl *a* distributions for the Kerguelen region. We use a weighted averaged merged product that is determined using the bio-optical model described by (Maritorena and Siegel, 2005). Data are distributed by the GlobColour project from the European Space Agency (http://hermes.acri.fr). The merged product is available on a 0.25° by 0.25° grid at daily and weekly (i.e. 8 day) time intervals, and it minimizes data gaps due to persistent cloud cover and low sun angles. These Chl *a* distributions illustrate the persistent high productivity that occurs on the Kerguelen Plateau and just to its east. Distributions during the KEOPS-2 cruise time period (Fig. 1c) are fairly typical of spring Chl *a* blooms shown in Fig. 1a.

BGD
11, 8373–8397, 2014

3 Methodology

In this study, we examine both the large-scale patterns of correlation between daily wind forcing and SST and also the longer-time-scale local, mesoscale modifications to these patterns. Several analyses have demonstrated a clear relationship between mesoscale SST features and surface winds (e.g., O'Neill et al., 2003, 2005). For example, O'Neill et al. (2003) showed that throughout the Southern Ocean, large SST gradients associated with narrow frontal features (with spatial scales of 10–100 km) have a significant impact on the overlying winds. The atmospheric boundary layer is less stable over warm water than cold water, and this induces greater vertical mixing of momentum and correspondingly higher surface winds over warm water than over cold water. O'Neill et al. (2003) showed that SST gradients thus induce cross-isotherm gradients in wind speed. For wind directed along isotherms, this leads to a non-zero wind-stress curl, which through Ekman pumping can drive localized vertical velocities, $w = \mathrm{curl}(\tau)/\rho f$, where τ is wind-stress, ρ is density and f is the Coriolis parameter. In the Southern Hemisphere, negative wind-stress curl induces upward Ekman pumping velocities (i.e. $w > 0$). For winds directed across isotherms, SST-induced modifications of the atmospheric boundary layer can induce a non-zero divergence of the wind stress.

For this study, we specifically evaluate the links between SST gradients and wind-stress curl or wind-stress divergence for the broad region surrounding the Kerguelen Plateau. We hypothesize that far from Kerguelen, mesoscale SST should influence wind-stress curl or divergence, but that close to Kerguelen this mechanism might break down. Our goal is to evaluate the geographic structure of the wind-stress curl/divergence dependence on SST in the Kerguelen region.

As O'Neill et al. (2003, 2005) noted, mesoscale wind-stress curl can vary substantially as a result of synoptic-scale weather disturbances. In order to minimize the impact of synoptic-scale storms, for some aspects of this analysis, data were averaged over three-month periods, corresponding to the typical decorrelation time-scales for oceanic eddies (Phillips and Rintoul, 2000). Wind speed, wind-stress curl, and SST all

BGD
11, 8373–8397, 2014

have large-scale meridional gradients, with significant gradients across the ACC fronts. For the three-month averaged data, a spatial filter was applied to remove scales larger than 10° latitude by 30° longitude from the data, in order to retain only mesoscale disturbances.

The variables analyzed in this study are interdependent. For example, SST and wind are both influenced by air–sea buoyancy fluxes, because of processes occurring in the atmospheric boundary layer that are not expected to influence nutrient upwelling. Thus for some components of this study we use partial correlations, which provide a formal mechanism to compute a correlation coefficient while controlling for the influence of additional variables (e.g., Prokhorov, 2001; Baba et al., 2004). Here partial correlations are applied to the unfiltered data.

4 Results

4.1 Assessing SST-wind relationships

Through most of the Southern Ocean, in year-round data high wind speeds correlate with cold SSTs, implying that wind-induced mixing deepens the mixed layer and brings cold water and nutrients to the surface (Kahru et al., 2010), and during spring and summer this can promote phytoplankton growth (Carranza and Gille, 2014). (In winter and early spring when stratification is low, high winds can deepen the mixed layer and move phytoplankton out of the euphotic zone, resulting in low Chl *a* (Kahru et al., 2010), but the focus of this study is on spring and summer.) Figure 2a shows partial correlations of unfiltered daily anomalies of wind speed and SST, controlled for the impact of surface heat fluxes. As hypothesized, wind speed and SST are negatively correlated (blue) almost everywhere, except in some locations to the north of Kerguelen. Positive correlations (red) fall along the Subantarctic Front and Polar Front of the ACC, which represent the primary axes of the current. In this region, changes in SST can feedback on the winds, and this manifests itself in regions of positive correlation.

BGD
11, 8373–8397, 2014

Wind-stress curl also influences SST throughout the Southern Ocean, although in different ways north and south of the zero wind-stress curl line. To the south of the zero wind-stress curl line, where negative wind-stress curl prevails, wind-stress curl is positively correlated with SST (red in Fig. 2b), implying that in most regions typical of Kerguelen, positive Ekman pumping (upwelling) events bring colder, more nutrient rich waters to the ocean surface. Along the axis of the ACC, to the north of Kerguelen, Fig. 2b shows patches of positive correlation, suggesting that SST impacts on wind may influence the correlation (even in this case, in which partial correlations have been used to control for surface heat flux).

An exception occurs in the Kerguelen wind shadow region, where high winds correlate with cold SSTs, but not necessarily high Chl *a* (not shown), implying that nutrient sources are somewhat different near the Kerguelen Plateau than they are in the open ocean.

When we filter to consider the impact of mesoscale eddies, we find that O'Neill et al.'s (2003) relationships between wind-stress curl, wind-stress divergence, and SST work well in open ocean areas but do not hold in the region just downwind of Kerguelen (Cambra, 2012). As an example for the time period corresponding to the KEOPS-1 field work, from December 2004 to February 2005, Fig. 3a shows the wind-stress curl and Fig. 3c shows the associated cross-wind component of the SST gradient. Figure 3b shows the wind-stress divergence, and Fig. 3d shows the down-wind component of the SST gradient. The wind-stress curl has elongated zonal structures, aligned along the main Southern Ocean fronts, which are reflected in the large spatial patterns of Fig. 3c, while the wind-stress divergence has isolated anomalies, generated around the large stationary meanders of the Southern Ocean fronts, which are reflected in the smaller-scale structure of the temperature gradient in Fig. 3d. Areas where the two components of the SST gradient are strongest, between 1.5×10^{-2} and 4×10^{-2} °C m^{-1}, correspond to the region of strong SST gradient and high EKE, calculated from geostrophic velocities from satellite altimetry, as shown in Fig. 3e. This occurs along the axis of the ACC, north and west of Kerguelen.

BGD
11, 8373–8397, 2014

In general the coupling between wind-stress curl and SST gradient is clearest in regions where EKE is greatest, and is less strong in regions of less intense EKE, close to Kerguelen. Figure 3f shows the zero-lag correlation coefficient between wind-stress curl and the cross-wind component of the SST gradient for the time period from 1 November 2002 through 31 October 2009. For Fig. 3f, 3-month time periods are used, and consecutive time windows overlap by 3 months, resulting in a total of 42 3-month periods. Because of the overlap, we assume the number of statistically independent samples to be two-thirds of 42, the 95 % significance level is 0.37, and correlation coefficients less than 0.37 are shaded light gray. The correlation coefficient is positive (red) and statistically significant for most of the region surrounding Kerguelen, consistent with the findings of O'Neill et al. (2003, 2005). Areas with high EKE in Fig. 3e, generally have statistically significant positive correlations in Fig. 3f, implying that the relationship identified by O'Neill et al. (2003, 2005) is present within the ACC, where EKE is moderate to high. In addition, Fig. 3f also indicates positive correlations to the north of the high EKE band in Fig. 3e and on the western side of the Kerguelen Plateau (around 48° S, 60° E), where EKE is less elevated. In contrast, to the southwest of the Kerguelen Plateau (south of 50° S and west of 70° E), the correlation between wind-stress curl and cross-wind SST gradient breaks down, possibly because the SST gradients (in Fig. 3c) are small, and their effect is not easily differentiated from noise.

Perhaps more surprising is that the coupling between wind-stress curl and the SST gradient is also low on the Kerguelen Plateau and due east of Kerguelen (around 48° S, 75° E), where SST gradients are nonetheless strong (Fig. 3c), and where we would normally expect to find high correlations. In these regions we hypothesize that the orography of Kerguelen itself may influence the wind-stress curl, and this topic will be addressed in the next section.

4.2 Impact of the Kerguelen wind-shadow

The 1850 m maximum elevation of the Kerguelen Islands is sufficient to generate a substantial wind shadow (Chelton et al., 2004). Downstream of Kerguelen, the wind

BGD
11, 8373–8397, 2014

shadow induces positive wind-stress curl to the south of the wind shadow and negative wind-stress curl to the north. Chelton et al. (2004) showed the structure of the wind shadow in the case of zonal winds. In reality in the Kerguelen region, wind direction is not strictly zonal, as illustrated in Fig. 4, which shows a probability density function of daily wind stress directions observed from the analysis period at 49.25° S, 71.25° E. (For these calculations, the unfiltered daily Ifremer/CERSAT stress fields were used.) Percentages in Fig. 4 indicate the fraction of the total days when wind was in the most frequent 30° sectors, with uncertainties computed as two standard deviations of 100 realizations of a bootstrap procedure with resampling. For example, 25 % ± 2 % of the time, winds were within ±15° of due east.

In order to evaluate the impact of the wind shadow in the region immediately surrounding Kerguelen, we sorted wind-stress curl data into bins on the basis of the prevailing wind direction to produce conditionally sampled mean wind-stress curl estimates, as shown in Fig. 5. The four panels of Fig. 5 correspond to 30° wind directional sectors, and black arrows show the prevailing wind direction for each panel. Regardless of the prevailing wind direction, a wind-stress curl dipole is established. For roughly westerly winds, negative wind-stress curl develops to the north of the wind shadow region and positive wind-stress curl to the south. This wind-shadow induced structure typically extends more than 200 km offshore from Kerguelen, extending across the Kerguelen Plateau. Figure 4 shows that more than 50 % of the time, winds are from the west or west-northwest, giving rise to the distinct pattern of negative wind-stress curl to the northeast of the Kerguelen Island, and positive wind-stress curl to the southeast, discussed by Chelton et al. (2004). This pattern also occurs in the December 2004 to February 2005 period shown in Fig. 3a.

Wind direction can shift rapidly, and many of the regions around Kerguelen are likely to experience both positive and negative wind-stress curl associated with the Kerguelen wind shadow. For example, in Fig. 5, the pixels at 49° S, 71° E, just to the east of Kerguelen, can have positive or negative wind-stress curl depending on the prevailing wind direction.

BGD
11, 8373–8397, 2014

Negative wind-stress curl is predicted to induce upward vertical Ekman pumping velocities. Due east of Kerguelen, where wind-stress curl is usually low, high Ekman pumping velocities might be expected to supply cold water and nutrients to the ocean surface, regardless of local temperature fronts or eddy processes. This Ekman pumping thus could explain the comparatively low correlation between the crosswind SST gradient and the wind-stress curl extending eastward from Kerguelen (around 48° S in Fig. 3f). Figure 5c shows a wind-shadow induced negative wind-stress curl east of Kerguelen, which coincides with consistently high Chl *a* blooms in Fig. 1. Southeast of Kerguelen, springtime Chl *a* is on average lower (Fig. 1a and c), coinciding with downward Ekman pumping with high variance in Fig. 5b and c. Thus this is consistent with the hypothesis that orographic wind-stress curl effects amplify upwelling of nutrients to the northeast of Kerguelen and reduce nutrient upwelling to the southeast of Kerguelen. Numerous other processes may also influence biological productivity on and downstream of the Kerguelen Plateau, including horizontal circulation over the sediment rich Kerguelen Plateau and eddy circulation associated with flow over and around the Plateau.

While the bulk of this analysis was carried out for the 2002–2009 time period when QuikSCAT winds and microwave SST are both available, we also evaluated the KEOPS-2 time period (see Fig. 1c and f) to check whether it was distinctive in any way from the main analysis period. In general, October–November wind conditions during the 2011 KEOPS-2 expedition were typical for the region. Details of the winds and Chl *a* differ from year to year, so that a formal statistical test, such as the Kolmogorov–Smirnov test, indicates that neither wind speed nor Chl *a* for any given year appears to be drawn from the same distribution as the climatology from all years combined together. Less stringent tests indicate that the October–November 2011 mean and standard deviation (for wind speed or for Chl *a*) are not statistically different from the means and standard deviations of individual years between October–November 2003 and 2009. Figure 6a shows a rose histogram for wind direction for October–November, 2011, color coded by speed. Prevailing wind directions during KEOPS-2 were consis-

BGD
11, 8373–8397, 2014

tent with prevailing wind directions shown in Fig. 4 for the 2002–2009 time period. In 2011, the largest daily average winds were oriented in the direction of most prevalent winds. Figure 6b shows the time-mean wind-stress curl for October–November, 2011. This is consistent with historical trends and indicates negative wind-stress curl, so upwelling favorable conditions, to the northeast of Kerguelen. For the KEOPS-2 time period, upwelling favorable conditions are slightly to the west of the maximum Chl *a* (Fig. 1c), suggesting that nutrients might be upwelled and then advected eastward by the prevailing winds or currents as the bloom develops.

5 Summary and discussion

This study has examined the mechanisms by which wind forcing can influence SST, and by extension nutrient availability, in the region around Kerguelen, where the KEOPS-2 field campaign was carried out. Although SST and satellite wind data are more limited in October–November 2011 than they are in earlier years, Chl *a* distributions in 2011 (Fig. 1c) are typical of climatological Chl *a* distributions in the region, suggesting that KEOPS-2 is a fairly typical year.

The findings of this study show that ocean response to wind in the Kerguelen region is characteristic of Southern Ocean areas south of the Polar Front and the zero-wind-stress curl line. High wind speeds correlate with cold SSTs (when controlled for air–sea fluxes), implying that wind mixing of the upper ocean entrains cold, nutrient-rich water into the mixed layer and the euphotic zone. In typical spring and summer conditions, this leads to high Chl *a* distributions. Negative wind-stress curl also correlates with cold SSTs, implying that upward Ekman pumping brings cold, nutrient-rich water to the surface. Air–sea feedbacks on the mesoscale modify these relationships, so that in most of the region around Kerguelen, we see evidence of a coupling between wind-stress curl and SST gradients, as O'Neill et al. (2003) described.

Exceptions to the expected relationships between wind-stress curl and SST gradients occur just to the east of Kerguelen, where the wind-stress curl is strongly influ-

BGD
11, 8373–8397, 2014

enced by the orographic wind shadow of Kerguelen's 1852 m summit. Persistent negative wind-stress curl just to the northeast of Kerguelen is expected to enhance upward Ekman pumping. Results show that the region of enhanced Ekman pumping coincides with the peak Chl *a* to the east of Kerguelen.

The magnitude of this wind-induced upwelling remains weak, with wind-stress curl of 2 to 5×10^{-7} N m^{-2} implying vertical Ekman pumping velocities w around 2–4×10^{-6} m s^{-1} giving a change of the thermocline of only 4–11 m month^{-1}. We note that the satellite-based wind fields have stronger amplitudes and variance than the global meteorological products (e.g. NCEP or ECMWF reanalysis winds). Even so, the gridded wind products we use may still be too smooth and may underestimate the effective wind-stress curl forcing in the region. Nonetheless, we expect larger upwelling and downwelling rates to be induced by the slope current's interaction with bathymetry, or within sub-mesoscale filaments generated by the turbulent flow.

The geographic co-location of the wind-induced upwelling in the Kerguelen wind shadow and the Chl *a* blooms suggests that although wind effects are comparatively weak, the wind is able to precondition the background stratification by supporting a shallower thermocline, allowing other processes to act more easily to bring iron and macronutrients to the euphotic zone. As Zhou et al. (2014) discuss, horizontal advection is also expected to play a key role in controlling nutrient availability and biological productivity in the euphotic zone. While many factors contribute to temperature and nutrient upwelling in the Southern Ocean, the results of this study suggest that wind-induced properties should be assumed to be a contributing factor in the Kerguelen region, and that the orographically modified wind-stress curl has the potential to be an important factor in explaining the location of the strong Chl *a* bloom to the east of Kerguelen.

Acknowledgements. This study has benefitted from informal discussions with numerous KEOPS-2 investigators. Wind data were obtained from the Centre de Recherche et d'Exploitation Satellitaire (CERSAT), at IFREMER, Plouzané (France). Microwave OI SST data are produced by Remote Sensing Systems and sponsored by National Oceanographic Part-

BGD
11, 8373–8397, 2014

nership Program (NOPP), the NASA Earth Science Physical Oceanography Program, and the NASA MEaSUREs DISCOVER Project. Data are available at www.remss.com. NASA's Research, Education and Applications Solution Network (REASoN) and MEaSURES programs funded development of the CCMP wind fields, which are distributed by the Physical Oceanography Distributed Active Archive Center (http://podaac.jpl.nasa.gov/). The altimeter products were produced by SSALTO/DUACS and distributed by AVISO with support from CNES (www.aviso.oceanobs.com). Chl *a* data are processed and distributed by ACRI-ST GlobColour service, supported by the EU FP7 MyOcean and ESA GlobColour Projects, using ESA ENVISAT MERIS data, NASA MODIS and SeaWiFS data. We gratefully acknowledge support from a NASA graduate student fellowship (MC), from NSF grants ANT-0948338 and OCE-1234473 (MC and STG), from NASA grants NNX08AI82G and NNX13AE44G (MC and STG), from the Observatoire Midi-Pyrénées (STG, RC and RM), and the CNES TOSCA programe (RC and RM).

References

Arrigo, K. R., Van Dijken, G. L., and Bushinsky, S.: Primary production in the Southern Ocean, 1997–2006, J. Geophys. Res., 113, C08004, doi:10.1029/2007JC004551, 2008. 8374

Atlas, R., Ardizzone, J., and Hoffman, R. N.: Application of satellite surface wind data to ocean wind analysis, in: Proc. SPIE, 7087, Remote Sensing System Engineering, San Diego, California, USA, 10 August, p. 70870B, doi:10.1117/12.795371, 2008. 8377

Atlas, R., Hoffman, R. N., Ardizzone, J., Leidner, S. M., and Jusem, J. C.: Development of a new cross-calibrated, multi-platform (CCMP) ocean surface wind product, in: AMS 13th Conference on Integrated Observing and Assimilation Systems for Atmosphere, Oceans, and Land Surface (IOAS-AOLS), 2009. 8377

Baba, K., Shibata, R., and Sibuya, M.: Partial correlation and conditional correlation as measures of conditional independence, Aust. NZ. J. Stat., 46, 657–664, 2004. 8380

Blain, S., Quéguiner, B., Armand, L., Belviso, S., Bombled, B., Bopp, L., Bowie, A., Brunet, C., Brussaard, C., Carlotti, F., Christaki, U., Corbière, A., Durand, I., Ebersbach, F., Fuda, J.-L., Garcia, N., Gerringa, L., Griffiths, B., Guigue, C., Guillerm, C., Jacquet, S., Jeandel, C., Laan, P., Lefèvre, D., Lo Monaco, C., Malits, A., Mosseri, J., Obernosterer, I., Park, Y.-H., Picheral, M., Pondaven, P., Remenyi, T., Sandroni, V., Sarthou, G., Savoye, N.,

BGD
11, 8373–8397, 2014

Scouarnec, L., Souhaut, M., Thuiller, D., Timmermans, K., Trull, T., Uitz, J., van Beek, P., Veldhuis, M., Vincent, D., Viollier, E., Vong, L., and Wagener, T.: Effect of natural iron fertilization on carbon sequestration in the Southern Ocean, Nature, 446, 1070–1074, 2007. 8374, 8375

Boyd, P. W.: Environmental factors controlling phytoplankton processes in the Southern Ocean, J. Phycol., 38, 844–861, 2002. 8374

Cambra, R.: Intéractions méso-échelles entre les vents et les tourbillons océaniques au large de Kerguelen, Master's thesis, Université Paul Sabatier, Toulouse, France, 40 pp., 2012. 8381

Carranza, M. M. and Gille, S. T.: Processes governing summer chlorophyll-a in the Southern Ocean, J. Geophys. Res., submitted, 2014. 8375, 8376, 8377, 8380

Chelton, D. B. and Wentz, F. J.: Global high-resolution satellite observations of sea-surface temperature for numerical weather prediction and climate research, B. Am. Meteorol. Soc., 86, 1097–1115, 2005. 8377

Chelton, D. B., Schlax, M. G., Freilich, M. H., and Milliff, R. F.: Satellite measurements reveal persistent small-scale features in ocean winds, Science, 303, 978–983, 2004. 8376, 8382, 8383

Chelton, D. B., Gaube, P., Schlax, M. G., Early, J. J., and Samelson, R. M.: The influence of nonlinear mesoscale eddies on oceanic chlorophyll, Science, 334, 328–332, 2011. 8375

de Baar, H. J. W., Boyd, P. W., Coale, K. H., Landry, M. R., Tsuda, A., Assmy, P., Bakker, D. C. E., Bozec, Y., Barber, R. T., Brzezinski, M. A., Buesseler, K. O., Boyé, M., Croot, P. L., Gervais, F., Gorbunov, M. Y., Harrison, P. J., Hiscock, W. T., Laan, P., Lancelot, C., Law, C. S., Levasseur, M., Marchetti, A., Millero, F. J., Nishioka, J., Nojiri, Y., Oijen, T. v., Riebesell, U., Rijkenberg, M. J. A., Saito, H., Takeda, S., Timmermans, K. R., Veldhuis, M. J. W., Waite, A. M., and Wong, C.-S.: Synthesis of iron fertilization experiments: from the Iron Age in the Age of Enlightenment, J. Geophys. Res., 110, C09S16, doi:10.1029/2004JC002601, 2005. 8374

Dibarboure, G., Pujol, M.-I., Briol, F., LeTraon, P., Larnical, G., Picot, N., Mertz, F., and Ablain, M.: Jason-2 in DUACS: updated system description, first tandem results and impact on processing and products, Mar. Geod., 34, 214–241, 2011. 8378

Ducet, N., Le Traon, P. Y., and Reverdin, G.: Global high resolution mapping of ocean circulation from the combination of TOPEX/POSEIDON and ERS-1/2, J. Geophys. Res., 105, 19477—19498, 2000. 8378

BGD
11, 8373–8397, 2014

Fauchereau, N., Tagliabue, A., Bopp, L., and Monteiro, P. M. S.: The response of phytoplankton biomass to transient mixing events in the Southern Ocean, Geophys. Res. Lett., 38, L17601, doi:10.1029/2011GL048498, 2011. 8375, 8376

Frants, M., Gille, S. T., Hatta, M., Hiscock, W. T., Kahru, M., Measures, C. I., Mitchell, B. G., and Zhou, M.: Analysis of horizontal and vertical processes contributing to natural iron supply in the mixed layer in southern Drake Passage, Deep-Sea Res. Pt. II, 90, 68–76, 2013. 8374

Freilich, M. H., Long, D. G., and Spencer, M. W.: SeaWinds: a scanning scatterometer for ADEOS II – Science overview, in: Proc. Int. Geoscience and Remote Sensing Symp., IEEE, Pasadena, CA, 960–963, 1994. 8377

Holm-Hansen, O., Kahru, M., Hewes, C. D., Kawaguchi, S., Kameda, T., Sushin, V., Krasovski, I., Priddle, J., Korb, R., Hewitt, R. P., and Mitchell, B. G.: Temporal and spatial distribution of chlorophyll-a in surface waters of the Scotia Sea as determined by both ship-board measurements and satellite data, Deep-Sea Res. Pt. II, 51, 1323–1331, 2004. 8374

Kahru, M., Mitchell, B. G., Gille, S. T., Hewes, C. D., and Holm-Hansen, O.: Eddies enhance biological production in the Weddell-Scotia Confluence of the Southern Ocean, Geophys. Res. Lett., 34, L14603, doi:10.1029/2007GL030430, 2007. 8374

Kahru, M., Gille, S. T., Murtugudde, R., Strutton, P. G., Manzano-Sarabia, M., Wang, H., and Mitchell, B. G.: Global correlations between winds and ocean chlorophyll, J. Geophys. Res., 115, 12040, doi:10.1029/2010JC006500, 2010. 8375, 8376, 8380

Korb, R. E., Whitehouse, M. J., Atkinson, A., and Thorpe, S. E.: Magnitude and maintenance of the phytoplankton bloom at South Georgia: a naturally iron-replete environment, Mar. Ecol.-Prog. Ser., 368, 75–91, 2008. 8374

Le Traon, P.-Y., Nadal, F., and Ducet, N.: An improved mapping method of multisatellite altimeter data, J. Atmos. Ocean. Tech., 15, 522–534, 1998. 8378

Lévy, M., Ferrari, R., Franks, P. J. S., Martin, A. P., and Rivière, P.: Bringing physics to life at the submesoscale, Geophys. Res. Lett., 39, L14602, doi:10.1029/2012GL052756, 2012. 8375

Mahadevan, A., D'Asaro, E., Perry, M.-J., and Lee, C.: Eddy-driven stratification initiates North Atlantic Spring phytoplankton blooms, Science, 337, 54–58, 2012. 8375

Maritorena, S. and Siegel, D. A.: Consistent merging of satellite ocean color data sets using a bio-optical model, Remote Sens. Environ., 94, 429–440, 2005. 8378

Martin, J., Gordon, R., and Fitzwater, S.: Iron in Antarctic waters, Nature, 345, 156–158, 1990. 8374

BGD
11, 8373–8397, 2014

Moore, J. K. and Abbott, M. R.: Phytoplankton chlorophyll distributions and primary production in the Southern Ocean, J. Geophys. Res., 105, 28709–28722, 2000. 8374

O'Neill, L. W., Chelton, D. B., and Esbensen, S. K.: Observations of SST-induced perturbations of the wind stress fields over the Southern Ocean on seasonal time-scales, J. Climate, 16, 2340–2354, 2003. 8375, 8379, 8381, 8382, 8385

O'Neill, L. W., Chelton, D. B., Esbensen, S. K., and Wentz, F. J.: High-resolution satellite measurements of the atmospheric boundary layer response to SST variations along the Agulhas Return Current, J. Climate, 18, 2706–2723, 2005. 8375, 8379, 8382

Phillips, H. E. and Rintoul, S. R.: Eddy variability and energetics from direct current measurements in the Antarctic Circumpolar Current south of Australia, J. Phys. Oceanogr., 30, 3050–3076, 2000. 8379

Planquette, H., Statham, P. J., Fones, G. R., Charette, M. A., Moore, C. M., Salter, I., Nedelec, F. H., Taylor, S. L., French, M., Baker, A. R., Mahowald, N., and Jickells, T. D.: Dissolved iron in the vicinity of the Crozet Islands, Southern Ocean, Deep-Sea Res. Pt. II, 54, 1999–2019, 2007. 8374

Pollard, R., Sanders, R., Lucas, M., and Statham, P.: The Crozet Natural Iron Bloom and Export Experiment (CROZEX), Deep-Sea Res. Pt. II, 54, 1905–1914, 2007. 8374

Prokhorov, A. V.: Partial correlation coefficient, in: Encyclopedia of Mathematics, edited by: Hazewinkel, M., Springer, ISBN 978-1-55608-010-4, 2001. 8380

Saha, S., Moorthi, S., Pan, H.-L., Wu, X., Wang, J., Nadiga, S., Tripp, P., Kistler, R., Woollen, J., Behringer, D., Liu, H., Stokes, D., Grumbine, R., Gayno, G., Wang, J., Hou, Y.-T., Chuang, H.-Y., Juang, H.-M. H., Sela, J., Iredell, M., Treadon, R., Kleist, D., Van Delst, P., Keyser, D., Derber, J., Ek, M., Meng, J., Wei, H., Yang, R., Lord, S., Van Den Dool, H., Kumar, A., Wang, W., Long, C., Chelliah, M., Xue, Y., Huang, B., Schemm, J.-K., Ebisuzaki, W., Lin, R., Xie, P., Chen, M., Zhou, S., Higgins, W., Zou, C.-Z., Liu, Q., Chen, Y., Han, Y., Cucurull, L., Reynolds, R. W., Rutledge, G., and Goldberg, M.: The NCEP climate forecast system reanalysis, B. Am. Meteorol. Soc., 91, 1015–1057, 2010. 8378

Venables, H. J., Pollard, R. T., and Popova, E. E.: Physical conditions controlling the development of a regular phytoplankton bloom north of the Crozet Plateau, Southern Ocean, Deep-Sea Res. Pt. II, 54, 1949–1965, 2007. 8374

Xue, Y., Huang, B., Hu, Z.-Z., Kumar, A., Wen, C., Behringer, D., and Nadiga, S.: An assessment of oceanic variability in the NCEP climate forecast system reanalysis, Clim. Dynam., 37, 2511–2539, 2010. 8378

BGD
11, 8373–8397, 2014

Zhou, M., Zhu, Y., d'Ovidio, F., Park, Y.-H., Durand, I., Kestenare, E., Sanial, V., Van-Beek, P., Queguiner, B., Carlotti, F., and Blain, S.: Surface currents and upwelling in Kerguelen Plateau regions, Biogeosciences Discuss., 11, 6845–6876, doi:10.5194/bgd-11-6845-2014, 2014. 8386

BGD
11, 8373–8397, 2014

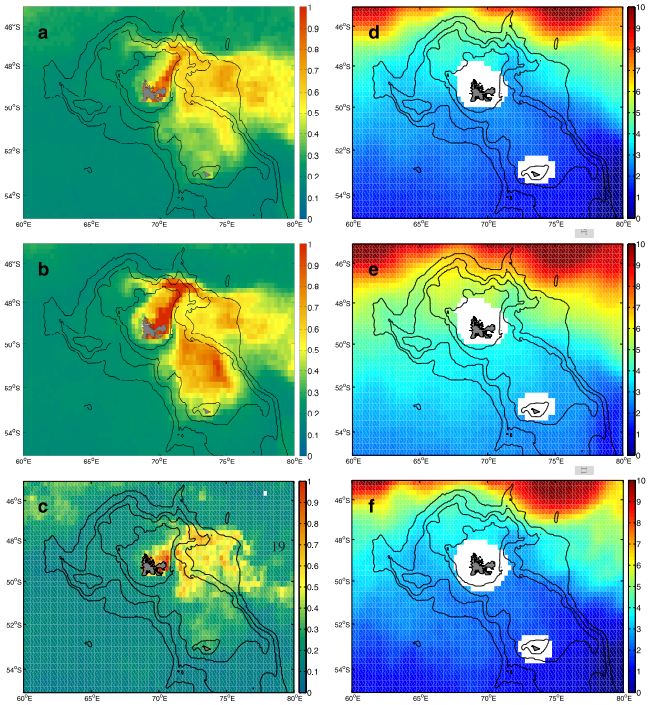

Figure 1. (a–c) Mean Chl *a* (in mg m^{-3}) for the Kerguelen region. **(a)** Climatological mean for the spring bloom, averaged over October, November, and December, 2000–2010. **(b)** climatological mean for the summer bloom (averaged over December, January, February, 2000–2010. **(c)** Mean for the KEOPS-2 research cruise, averaged over October and November 2011. Because Chl *a* is log-normally distributed, here the mean is computed as exp(mean(log(Chl *a*))), where log refers to the natural log. **(d–f)** Mean SST (in $^{\circ}$C) for the Kerguelen region. **(d)** for October, November, December, as in **(a)**; **(e)** for December, January, February, as in **(b)**; **(f)** for October–November 2011, as in **(c)**. In this figure and subsequent figures, bathymetry is contoured at 3000, 2000, 1000, and 200 m depth.

BGD
11, 8373–8397, 2014

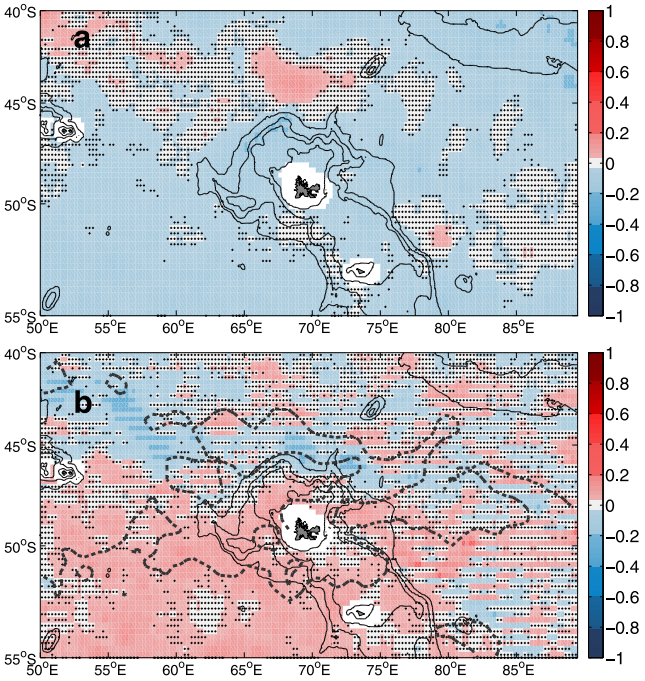

Figure 2. Partial correlation coefficients for **(a)** wind speed vs. SST and **(b)** wind-stress curl vs. SST, in both cases controlled for surface heat flux. Partial correlations are computed for the spring and summer growing season only, from September to February. In **(a)** blues indicate that positive wind anomalies are associated with cold SSTs, and in **(b)** reds in the region adjacent to Kerguelen indicate that negative wind-stress curl is linked to cold SSTs. Pixels are cross-hatched where the correlation coefficient is not statistically significant at the 95 %. Black dashed line indicates the climatological mean zero-wind stress curl line; negative wind-stress curl occurs south of the zero-wind stress curl line (and within closed contours to the north) and corresponds to upward vertical Ekman pumping.

BGD
11, 8373–8397, 2014

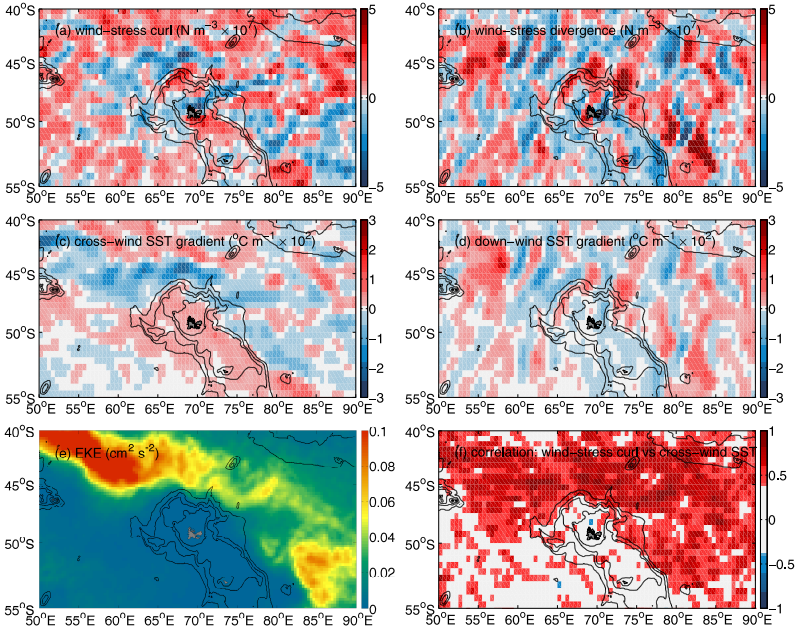

Figure 3. (a) Wind-stress curl (in N m^{-3} × 10^7) for December 2004 to February 2005, spatially filtered to remove large-scale signal, as discussed in the text. **(b)** Wind-stress divergence (in N m^{-3} × 10^7) for the same time period, also spatially filtered. **(c)** Crosswind components of the SST gradient (in °C m^{-1} × 10^2) derived from QuikSCAT wind data and AMSR-E microwave SST. SST gradients are filtered spatially using a 10° × 30° window, averaged over the period from December 2004 to February 2005. Isobaths are plotted at 200 m and at 1000 m intervals. **(d)** Downwind component of SST gradient (in °C m^{-1} × 10^2), computed the same way as in **(c)**. **(e)** Eddy kinetic energy derived from satellite altimetry, showing high eddy kinetic energy to the north of Kerguelen, along the core of the Antarctic Circumpolar Current. **(f)** Correlation between wind-stress curl and the crosswind component of the SST gradient, computed using 42 3 month samples, with consecutive samples overlapping by one month. White areas are not statistically significant at the 95 % level.

BGD
11, 8373–8397, 2014

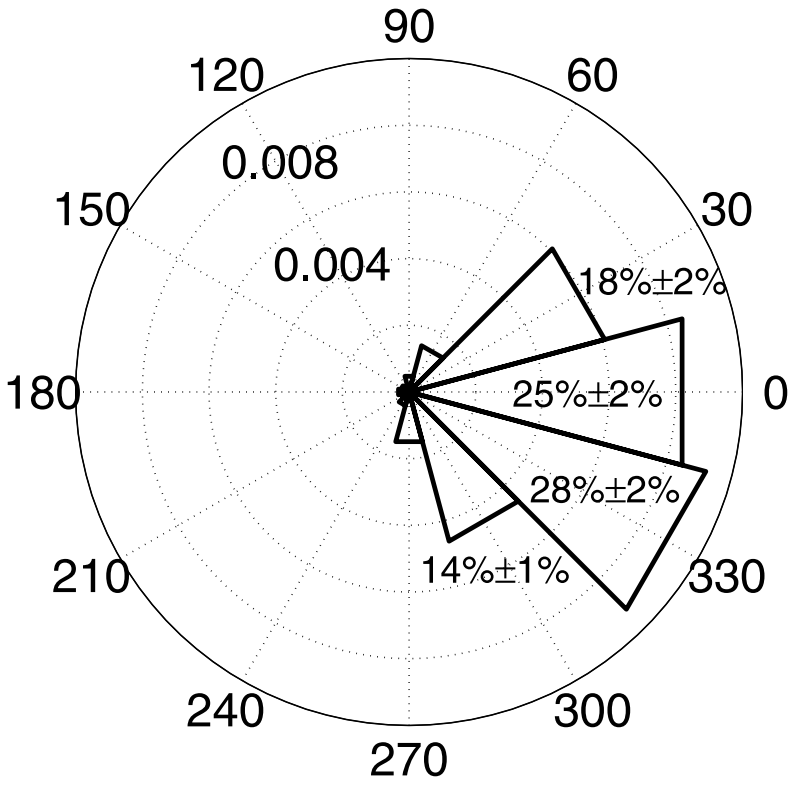

Figure 4. Probability density function of wind direction at 49.25° S, 71.25° E, just to the east of Kerguelen. The pdf is represented as a rose histogram, appropriately normalized so that the representation is not dependent on bin width or sample size. A total of 2522 daily wind observations are used. Also indicated are the percentages of days in which winds fall into each of the four most common directional bins, with 2σ uncertainties determined from a 100-realization bootstrap with resampling.

BGD
11, 8373–8397, 2014

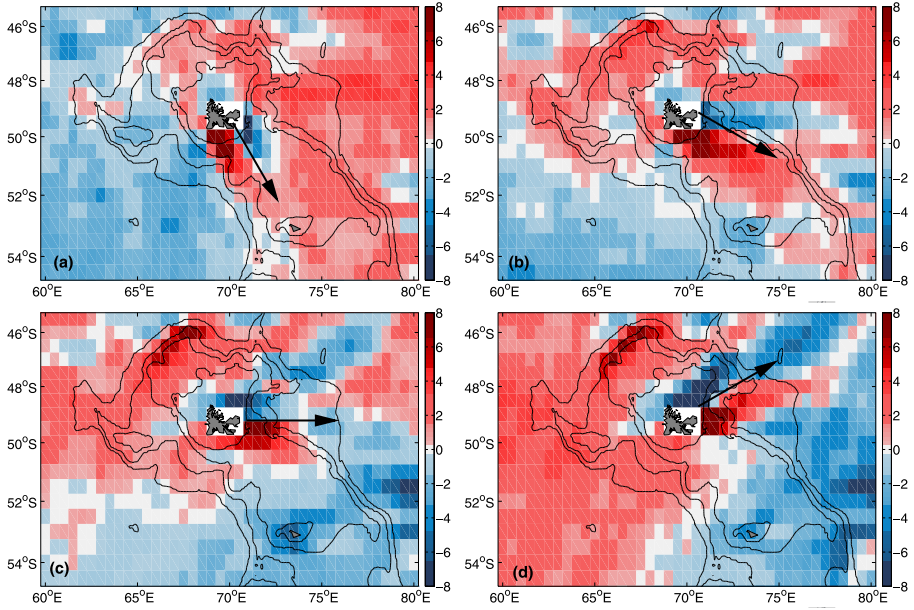

Figure 5. Wind-stress curl (in 10^{-7} N m^{-3}), sorted by prevailing wind direction for winds **(a)** from −75° to −45°, **(b)** from −45° to −15°, **(c)** −15° to +15°, and **(d)** +15° to +45°. Contours indicate the 200 m, 1000 m, 2000 m, and 3000 m isobaths. Black arrows indicate the prevailing wind direction for each panel. (The maps use Mercator projection so angles on the map correspond to geographic angles.)

BGD
11, 8373–8397, 2014

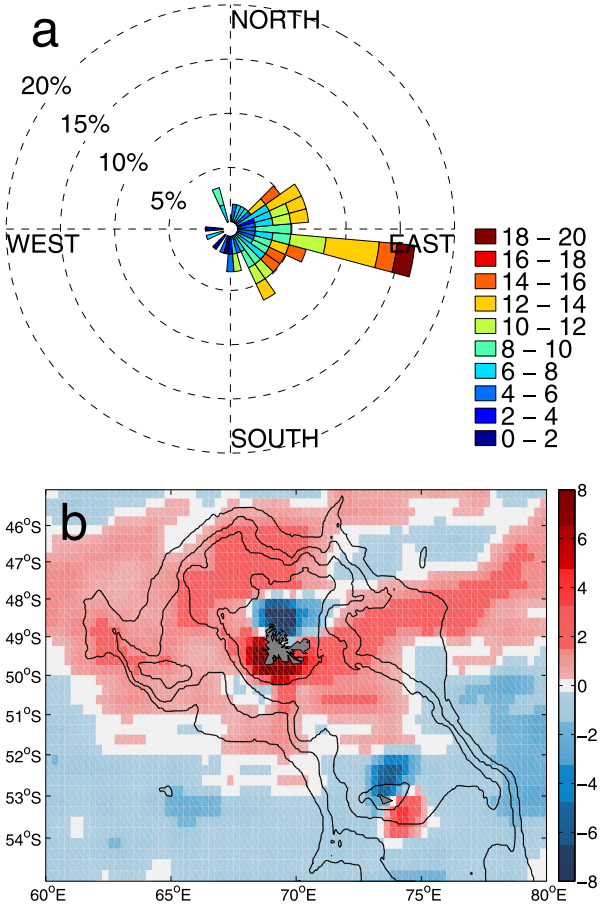

Figure 6. (a) Rose histogram for daily wind direction and speed (colors, in $m\,s^{-1}$) in October and November 2011, during the KEOPS-2 expedition. **(b)** Wind-stress curl (in $10^{-7}\,N\,m^{-3}$) in October and November 2011. Winds are derived from the CCMP product.

BGD
11, 8373–8397, 2014